Decoding-based Regression

Anonymous authors
Paper under double-blind review

Abstract

Language models have recently been shown capable of performing regression wherein numeric predictions are represented as decoded strings. In this work, we provide theoretical grounds for this capability and furthermore investigate the utility of causal auto-regressive sequence models as numeric prediction heads given any feature representation. We find that, despite being trained in the usual way - for next-token prediction via cross-entropy loss - decoder-based heads are as performant as standard pointwise heads when benchmarked over standard regression tasks, while being flexible enough to capture smooth numeric distributions, such as in the task of density estimation.

1 Introduction

Despite being originally developed for the purpose of text generation and chat applications, large language models (LLMs) have recently been applied for new applications, one of which is regression tasks, and more broadly the prediction of numeric outcomes. Vacareanu et al. (2024) have shown service-based LLMs such as ChatGPT and Gemini capable of regression with performance comparable to that of traditional regression methods such as random forests, while Song et al. (2024) have shown smaller T5-based models can be trained specifically on large amounts of regression data for strong transfer learning.

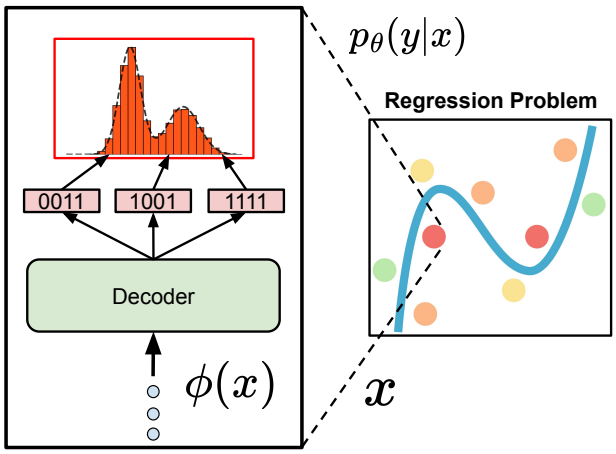

Figure 1: Given any feature representation $\phi(x)$, we attach a decoding-based head to output predictive distribution $p_\theta(y|x)$.

For input-output pair (x, y), where x is a feature vector and y is a real number, a regression model's performance is determined by two factors: how it processes x and how it models the output y – e.g. the representation of y as well as distributional assumptions on $p(y|x)$. While the mentioned previous works (Vacareanu et al., 2024; Song et al., 2024) in *text-to-text regression* can be seen as cases where both representations are based on tokens, this combination is not necessarily required. Tang et al. (2024) investigate the isolated case where LLM embeddings of x are attached to traditional numeric tensor heads, while Nguyen et al. (2024) investigate the case when embeddings for x are eventually attached to Gaussian distribution heads. Both can be seen as particular instances when x is represented as text, but traditional regression heads are still used. However, there has not been work investigating the inverse case when x is represented using standard numeric feature vectors but y is represented as text, i.e. using decoding-based regression heads alone, where for example, 1.23 is represented as `<1><.><2><3>`, despite this style of tokenization being used in several works training language models for specific numeric tasks, such as arithmetic (Nogueira et al., 2021), linear algebra (Charton, 2022), and symbolic regression (d'Ascoli et al., 2022).

In contrast to traditional numeric or even parameterized distribution (e.g. Gaussian) heads, decoding-based heads may be much more flexible, as they can represent any numeric distribution approximately over $\mathbb{R}$ without the need for explicit normalization. However, due to their initial lack of inductive bias over numeric distances, numeric token representations and sequential dependencies may need to be learned using more training data, and thus it is worth empirically investigating these trade-offs in isolated, controlled experiments. Our research provides valuable insights on using numbers as an output modality of token-based autoregressive decoders.

Our contributions are thus as follows:

- We formalize decoding-based regression by specifying its tokenization scheme, proving how well it can fit arbitrary smooth one-dimensional densities under some assumptions, and exploring methods for pointwise estimation.
- We empirically demonstrate that with the right settings, decoding-based regression heads are data-efficient and competitive with regular pointwise heads over numerous tabular regression tasks, and are also expressive enough to match Gaussian mixture models for density estimation tasks.

2 Related Work and Motivation

The idea of *text-to-text regression* is especially relevant as LLMs are currently being fine-tuned as "Generative Reward Models" (Mahan et al., 2024; Zhang et al., 2024), i.e. end-to-end scoring methods for reinforcement learning feedback (Ziegler et al., 2019; Bai et al., 2022) or LLM-as-a-Judge (Zheng et al., 2023). Such reward modeling methods can be simpler than other forms such as Bradley-Terry (Bradley & Terry, 1952) which requires appending additional prediction heads and custom losses. However, little analysis has been done in isolation on the theoretical and modeling capabilities of using text, or more generally tokens, to represent floating point numbers. Understandably, one could argue that regular supervised fine-tuning over numbers represented as strings is unprincipled, considering that there is no notion of numeric distance when using cross-entropy loss.

However, we argue that this approach is actually a natural outcome of observed phenomena and techniques proposed in recent works. Given a post-processed representation $\phi(x) \in \mathbb{R}^d$ after x is sent through a task-specific encoder (MLP, CNN, etc.), we provide an overview of relevant work on various regression heads which can be applied on top of $\phi(x)$ to return numeric outputs, with additional techniques in Appendix C.

Tensor-based Representations: By far, the most commonly used regression head is a a learnable deterministic projection of $\phi(x)$ to a scalar, with optional transformations that may be performed afterwards; e.g. Bradley & Terry (1952) can be seen as appending an additional sigmoid head to enforce the raw outputs to be within $[0, 1]$. All such cases require y-values to be in a normalized space, to allow stability during training. We term these types as *pointwise* heads.

In the case of probabilistic outputs, one may apply parametric distribution heads such as Gaussians, e.g. $p(y|x) = \mathcal{N}(\mu, \sigma^2)$ where μ, σ are learned projections over $\phi(x)$. However, these apply heavy assumptions on the underlying output distribution, which may not hold true in real world cases. One can extend the head to be a finite (Bishop, 1994) or even infinite (Rasmussen, 1999) mixture of Gaussians to increase flexibility. Such mixture techniques can be more broadly seen within the realm of density estimation (Parzen, 1962; Rosenblatt, 1956) in which a complex distribution may be estimated using multiple simpler basis distributions.

Histogram (Riemann) Distribution Heads: One such basis common in deep learning applications is the piece-wise constant basis, for learning histograms over a finite support set $\{y_1, \ldots, y_n\} \subset \mathbb{R}$ via softmax parametrization, i.e. $p(y_i|x) = \text{Softmax}^{(i)}(\phi(x)^T \cdot w)$, which has led to strong results in value-based reinforcement learning (Imani & White, 2018; Bellemare et al., 2017) and tabular data (Hollmann et al., 2025; Chen et al., 2022). However, a drawback is that learning numeric distances between all of the bins requires more data as the size of the vocabulary increases. We define these as *Riemann* heads.

While there have been works on ordinal regression to learn rankings among these bins, such as using rank-consistency (Cao et al., 2020) and soft labels / metric-awareness (Diaz & Marathe, 2019), we propose a

much simpler way, by simply considering the histogram distribution as a special length=1 case of decoding a sequence. By extending the sequence length instead, there can be an exponential reduction in bin count - e.g. 1000 (=10^3) bins can be expressed instead using 10 bins and 3 decoding steps. While this intuitive idea has been studied in extreme classification problems (Wydmuch et al., 2018), it has not been thoroughly examined for numeric regression, which is the focus of our work.

3 Decoding-Based Regression

3.1 Preliminaries

In a standard regression problem (generalized for probabilistic outputs), we assume there exists some underlying conditional distribution $p(y|x)$ and with $y \in \mathbb{R}$, and we additionally assume there already exists an encoding $\phi(x)$ specific to the task for learning features, and our focus is to understand the effects of modeling the output y, after utilizing training data $\{(X_i, Y_i)\}_{i=1}^N$.

3.2 Token-Based Representation

We now formalize the representation of floating point numbers as a sequence of tokens. Given a vocabulary of all possible tokens $\mathcal{V}$, we define a *token representation* as a mapping from $y \in \mathbb{R}$ to fixed-length sequence of tokens $(t_1, \ldots, t_K) \in \mathcal{V}^K$. Since the token space is finite while $\mathbb{R}$ is uncountable, this mapping is lossy (i.e. not invertible) and introduces a notion of *rounding error*. We can apply a *decoding-based regression head*, represented as auto-regressive prediction model $p_\theta(t_k \mid \phi(x), t_1, \ldots, t_{k-1})$ from which we may thus obtain an end-to-end model $p_\theta(y|x) = p_\theta(t_1, \ldots, t_K \mid \phi(x)) = \prod_{k=1}^K p_\theta(t_k \mid \phi(x), t_1 \ldots t_{k-1})$.

Normalized Tokenization: If y is restricted to $[0, 1]$ (via scale normalization for example), then we show we can represent any smooth density $p(y|x)$ with an increasing level of granularity as more tokens are used in the numeric representation, under some "universality" assumptions on p_θ. This can be seen intuitively with a tree-based construction, i.e. for a base B, the vocabulary contains <0>, <1>, ..., <$B-1$>, and y is simply represented by its base-B expansion up to a length K. This setting aligns with standard data-science practices of also normalizing y-values according to training data or known bounds.

Unnormalized Tokenization: However, there are cases in which we would like to use an *unnormalized* tokenization scheme. Such cases include multi-task regression, in which different tasks may have varying y-scales, or expressing very wide y-ranges for which appropriately normalizing y-values for the correct balance between numeric stability and expressiveness would be very tedious.

In this case, we may simply view normalized tokenizations as "mantissas" and then left-append sign and exponent tokens to form a base-B generalization of the common IEEE-754 floating point representation (IEEE, 2019). Given length parameters E and M, our tokenization is therefore <s><s_e><e_1>...<e_E><m_1>...<m_M> where $s_e, e_1, e_2, \ldots, e_E$ are the sign and base-B representation of the exponent and $m_1, m_2, \ldots, m_M$ are the most significant base-B digits of the mantissa. E.g. if (B=10, E=3, M=4), then $10^{-222} \times 1.23456789$ will be represented as <+><-><2><2><2><1><2><3><4>. Signs <s>, <s_e> can have their own dedicated <->, <+> tokens or optionally reuse the <0>,<1> tokens from $\mathcal{V}$; this made little difference in results.

Note that the vocabulary can additionally contain "special" tokens for representing outputs not within a supported numeric range. For example, one can use a token <NaN> to represent non-numbers, commonly used in cases where x may be an invalid input. We mention such cases for useful downstream applications, although the scope of this paper assumes y is always within $\mathbb{R}$.

Architecture: Any autoregressive model can be used, so long as it supports constrained token decoding to enforce proper sequences which represent a valid number. By default, we use a small Transformer (Vaswani et al., 2017) due to its strong autoregression capabilities, with the initial token embedding as $\phi(x)$. As we show in our experiment section, this Transformer size can be made minimal, with negligible contribution to parameter count in comparison to the encoder.

For large enough base B and sequence lengths (both normalized and unnormalized), practically any y-value will be within the expressible range and rounding errors will be minimal. However, the trade-off

is that the vocabulary size and sequential dependencies between tokens will also increase, and learning better numeric representations may thus require more training data. While it's possible to first pretrain these numeric representations as in Hollmann et al. (2025) for the histogram distribution, we show that with proper hyperparameter tuning, the Transformer decoder can be used out-of-the-box as a randomly initialized regression head.

3.3 Pointwise Estimation

In many cases, one may only be interested in a scalar quantity of interest $M(p_\theta)$ of the model's distribution (e.g. its mean). If p_θ matches the true distribution p perfectly, then for a given pointwise loss $\ell : \mathbb{R}^2 \to \mathbb{R}$ the goal is then to select $M(p)$ which minimizes $\mathbb{E}_{y\sim p(\cdot|x)}\left[\ell(M(p), y)\right]$. For common error functions such as ℓ_2, ℓ_1, and ℓ_0, it is well known that the optimal values are the mean, median, and mode of $p(\cdot|x)$ respectively, an observation which Lukasik et al. (2024) also use to improve LLM decoding.

To estimate these $M(p)$, the mode can be approximated using e.g. beam search (Graves, 2012), but efficiently estimating other common general pointwise representatives $M(p)$ from pure temperature samples is a broad topic - for example, one can efficiently approximate the true median from the Harrell-Davis estimator (Harrell & Davis, 1982), and more generally we refer the reader to Lehmann (1983) on statistical point estimators.

Especially for unnormalized tokenization, additional care needs to be taken, since in practice, the model can have a miniscule but non-zero probability of decoding an arbitrarily large outlier, even if the underlying true distribution is bounded. Such outliers can easily sway non-robust estimators such as the sample mean, as observed in Song et al. (2024). This issue fundamentally comes from the fact that some tokens are more significant than others, prompting the use of alternative tokenizations based on coding theory which are robust to corruptions, which we show can be effective in our experiment section.

Alternatively, decoding techniques from the LLM literature can also be used, e.g. top-k (Fan et al., 2018) or top-p (Holtzman et al., 2020), or even simply decreasing the temperature to increase model confidence and thereby filter out possible outliers. One can also avoid decoding altogether and use recently proposed RAFT (Lukasik et al., 2025; Chiang et al., 2025) which estimates $M(p)$ using a query-based approach using a finite fixed evaluation set $\mathcal{Y}$, e.g. for mean, $\mathbb{E}_{y\sim p_\theta}[y] \approx \frac{1}{N}\sum_{y'\in\mathcal{Y}} p_\theta(y')\cdot y'$, although the choice of $\mathcal{Y}$ may be non-trivial to obtain an unbiased estimate, especially over unnormalized tokenizations. This may also defeat the purpose of using a decoder head, which offers several density estimation benefits, as we discuss below. Overall, the choice of method for computing pointwise representations we leave as a hyperparameter to be tuned depending on the application.

3.4 Density Estimation and Theory

During training, to allow the full probabilistic modeling benefits of using a decoder head, we apply the standard cross-entropy loss over all sequence tokens. For a model p_θ and target $y = (t_1, \ldots, t_K)$, the cross-entropy loss (omitting x to simplify notation) will be:

$$H(y, p_\theta) = \sum_{k=1}^{K} \sum_{\widehat{t_k}\in\mathcal{V}} -\mathbb{1}(\widehat{t_k} = t_k) \log p_\theta(\widehat{t_k}|t_1, \ldots, t_{k-1})$$

The expected loss over all y sampled from the true distribution is then $\mathbb{E}_{y\sim p}\left[H(y, p_\theta)\right]$.

Given our tree-based tokenization and training loss, we provide formal guarantees for estimating one-dimensional densities on $[0, 1]$. Note that densities with finite support can be shifted and rescaled to have support in $[0, 1]$. Define $\lambda_k : [0, 1) \to \{0, 1\}^k$ be the operation that returns the first k bits after the radix point in the (possibly infinite) binary representation of y. Concretely, if $y = 0.b_1b_2b_3b_4...$ then $\lambda_k(y) = (b_1, \ldots, b_k)$. We abuse notation and interpret λ_k's output either as a sequence or as the real number it represents ($\sum_{i=1}^{k} b_i 2^{-i}$) depending on the context. The analysis is presented using binary (base-2) representations (e.g. $\mathcal{V} = \{0, 1\}$) for simplicity, but it holds for arbitrary bases. First, we define an assumption on the learnability of our model.

Definition 1 (K-bit universality)**.** *Let $H(p,q) = \mathbb{E}_{y\sim p} - \log q(y)$ denote the cross-entropy between discrete distributions p and q. Note that $H(p,p)$ is just the Shannon entropy of p. Call parametric model p_θ K-bit universal if for all discrete distributions p on K-bit strings (equivalently, 2^K categories),*

$$\min_\theta H(p, p_\theta) = H(p,p).$$

In other words, p_θ is K-bit universal if it is flexible enough to fit any discrete distribution on 2^K categories.

We now give our main result below, expressing the distributional fit in terms of bias and variance. The proof is deferred to Appendix B.

Theorem 1. *Assume our decoding-based regression model $p_\theta : \{0,1\}^K \to \Delta^{2^K}$ is K-bit universal. Furthermore, define p_θ^k as probability of the first k bits under p_θ, marginalizing out the remaining bits. Concretely,*

$$p_\theta^k((b_1,\ldots,b_k)) = \sum_{\{b_{k+1},\ldots,b_K\}} p_\theta((b_1,\ldots,b_K)).$$

Seen another way, p_θ^k is the distribution over k-bit strings that results from auto-regressive decoding p_θ for exactly k steps.

Now let $f : [0,1] \to \mathbb{R}$ be any twice continuously differentiable density function. With $\{Y_1,\ldots,Y_N\}$ as i.i.d. draws from f, define θ^* as the maximum likelihood estimator on the truncated sequence of K bits. Concretely,

$$\theta^*(Y_1,\ldots,Y_N) = \operatorname*{argmin}_\theta \frac{1}{N}\sum_{n=1}^{N} -\log p_\theta(\lambda_K(Y_n)).$$

*Define **risk** R as the **mean integrated squared error** between true density f and an estimator $\widehat{f}_N(Y_1,\ldots,Y_N)$:*

$$R(f,\widehat{f}_N) = \mathop{\mathbb{E}}_{Y_1,\ldots,Y_N\sim f} \int_0^1 \left(f(y) - \widehat{f}_N(y)\right)^2 dy.$$

Define density $f_N^{k*}(y) = 2^k p^k_{\theta^*(Y_1,\ldots,Y_N)}(\lambda_k(y))$ for $y \in [0,1]$. Then we have,

$$R\left(f, f_N^{k*}(y)\right) = \underbrace{\frac{2^{-2k}}{12}\int_0^1 f'(y)^2 dy}_{Bias} + \underbrace{\frac{2^k}{N}}_{Variance} + \underbrace{O(2^{-4k} + 1/N)}_{Negligible}, \quad \forall k \le K.$$

Note that this theorem is a broad statement, applicable to Riemann heads and decoders even if they perform inference at a lower token length k than the maximum length K used during training. For simplicity, let us assume that decoding and training use the same length (i.e. $k = K$). Intuitively, this implies that one needs a higher resolution K to capture the curvature of f, but as the number of bins increases, more data points N are required to learn to separate these 2^K bins. In Figure 2, for large N=16384, we show this trend holds empirically where there is an optimal $K\approx5$ which minimizes the error.

When N is quite small (e.g. 1024) we see that the decoder significantly deviates from the theoretical risk (for the better) when the number of bits is large (>9), while the Riemann still fits it tightly. Recall that we required a "universality" assumption, which says that our model can learn any discrete distribution over K-bit strings perfectly. We can decompose this assumption further into two pieces: 1) that there exists θ^* in our model class that achieves the minimum cross-entropy (i.e. $p_{\theta^*} = p$ in Definition 1), and 2) that our SGD-based training procedure is able to find it. An explanation for this phenomenon is that in this regime (low sample size and large number of bits, or equivalently, a large number of bins), the risk profile of the classical Riemann estimator is dominated by the variance term. Few samples land in each bin and as a result the histogram-based density estimate for the bins is noisy.

It is conceivable that a combination of the inductive bias of our model class and the implicit bias of our SGD training procedure makes the decoder less likely to fit noise; a concrete example would be that the

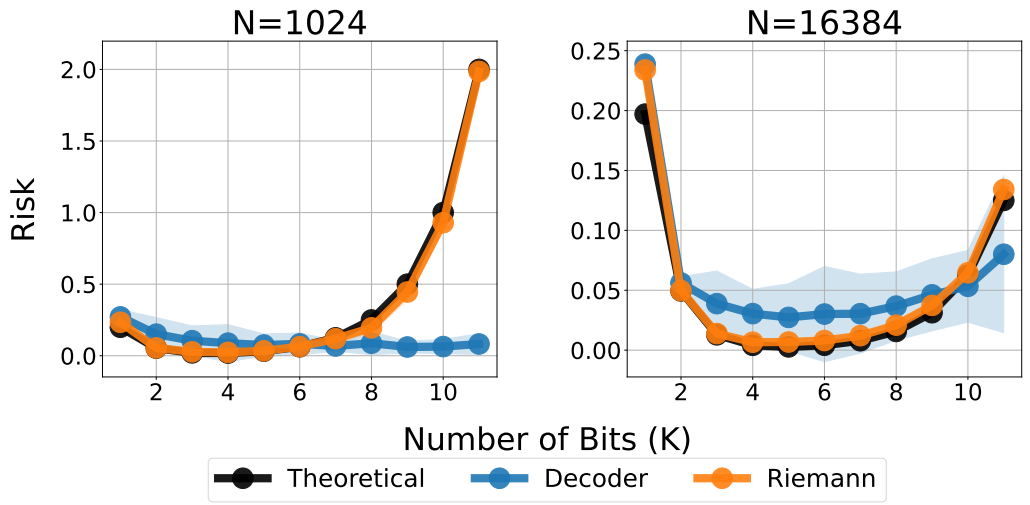

Figure 2: Lower (↓) is better. Risk (theoretical and empirical) when varying K and N to fit a truncated $\mathcal{N}_{[0,1]}(0.5, 0.25^2)$ distribution using binary tokenization. Results averaged across 10 runs each.

model is biased to learn smooth distributions, and so when asked to fit the highly discontinuous empirical distribution arising from dropping few samples into a large number of bins, it refuses to, instead opting to learn a smooth approximation, and thereby driving down the variance term and hence the overall risk. This suggests the decoder possesses implicit regularization properties which make it much more efficient with low training data.

Taking a closer look at the decoding mechanism, a crucial observation is that λ_k essentially discretizes the unit interval (and hence f as well) into bins $\{B_j\}_{j=0}^{2^k-1}$, where $B_j = [j2^{-k}, (j+1)2^{-k})$ so that $\mathbb{P}(x \in B_j) = \int_{B_j} f(y)dy$. We can identify k-bit sequence $y = 0.b_1 \dots b_k$ with the interval $[y, y + 2^{-k}]$. With a single bit ($K = 1$) we learn a histogram estimator on two bins $[0, 1/2)$ and $[1/2, 1)$ representing 0 and 1. With two bits we refine our prediction using four bins: $[0, 1/4)$, $[1/4, 1/2)$, $[1/2, 3/4)$, and $[3/4, 1)$ representing $(0, 0), (0, 1), (1, 0), (1, 1)$ respectively (because, for example $(0, 1)$ means $0.01_2 = 1/4$).

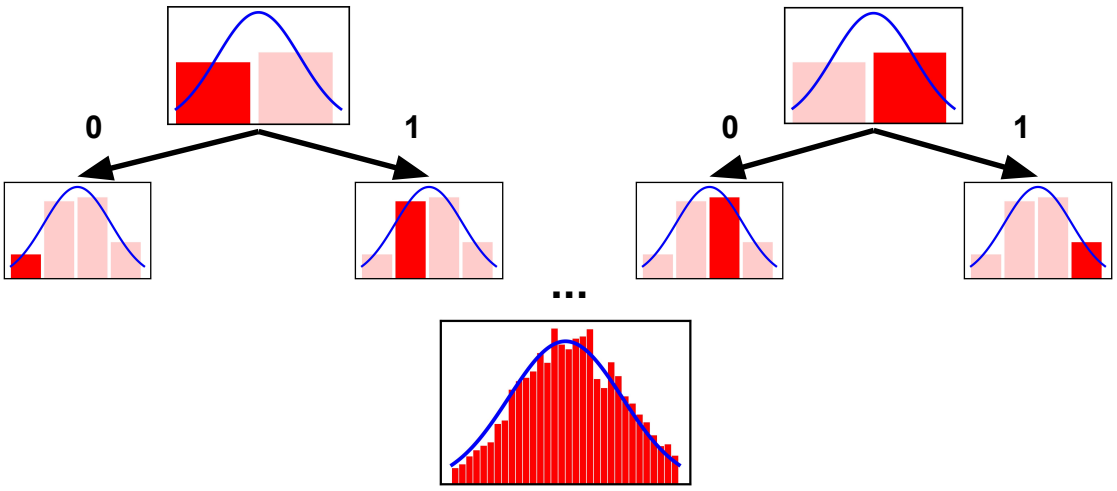

Figure 3: Visualization of fitting a truncated Gaussian distribution. Each level k of the binary tree represents the empirical fit using k bits, and each bin gets subdivided into two.

We can interpret binary representations in terms of binary trees on 2^K leaf nodes where nodes represent intervals (the root representing $[0, 1)$) and left and right children represent the left and right halves of

the node's interval. Reading off bits tells us how to traverse this tree, where 0 and 1 mean traverse the left and right subtrees respectively. For example, to arrive at $(0, 1, 1) = 0.011_2 = 3/8$ our traversal is: $[0, 1) \to [0, 1/2) \to [1/4, 1/2) \to [3/8, 1/2)$.

When trained on K-bit sequences, our decoder model p_θ *simultaneously* learns K histogram estimators for f; $2^k p_\theta^k(\lambda_k(y))$ is the k-th histogram estimator (over 2^k bins). In other words, as we decode bits one-by-one auto-regressively, we are iteratively refining our prediction. Figure 3 shows this mechanism in detail in the case of fitting a truncated Gaussian distribution.

There are alternatives to binary representations, for example *p-adic expansions*, or even the *Stern–Brocot tree* which uses the mediant to determine the child-parent relationship. An interesting research question left for future work is whether these more exotic representations of real numbers are better suited for our sequence-based regression model than the standard representations.

4 Experiments

Our main goals for experiments are to:

- Demonstrate decoders can be effective swap-in replacements to common pointwise regression heads.
- Establish the density estimation capabilities of the decoding-based head over any distribution over $\mathbb{R}$.
- Ablate the effect of decoder size and sequence-specific methods such as error correction on performance.

To maintain fairness and minimize confounding factors, all neural network methods have access to the same encoder $\phi(x)$, which is a large multi-layer perceptron (MLP) with ReLU activations, with hyperparameter sweeps over number of layers (up to 5) and hidden unit sizes (up to 2048). This minimizes the decoding head's contribution to representation learning (as opposed to numeric modeling), since it will be relatively negligible in size to $\phi(x)$, i.e. less than 10% of the total network parameter count.

Furthermore, for distributional baselines (e.g. decoder, Riemann), we sweep their specific settings (e.g. number of bins / tokenization) over reasonable values - additional details are found in Appendix D. For the vast majority of tabular regression problems, we found that the process of training and tuning only requires at most 20 minutes on a single Nvidia P100 GPU, making the decoder head relatively cheap to use. For comparisons, we use relative mean squared error within individual tasks and scale-invariant Kendall-Tau correlation for aggregate comparisons.

4.1 Curve Fitting

We begin by visually demonstrating the fundamental representation power of tokenization. In Figure 5, the unnormalized decoder is able to successfully capture the shapes of various functions with which the pointwise head struggles, even with unbounded training data. The issue with using the pointwise head stems from two main factors: (1) requiring y-normalization, which leads to numeric instabilities especially with functions with very high or unbounded y-ranges, and (2) struggling to model high rates of change (i.e. large Lipschitz constants). In contrast, the unnormalized decoder does not encounter these issues due to its ability to express a very high range of y-values.

	Input Dimension			
Regression Head	**5**	**10**	**15**	**20**
Unnormalized Decoder	89	88	87	86
Normalized Decoder	89	88	86	86
Pointwise	89	88	88	86
Riemann	88	88	87	86

Figure 4: Higher (↑) is better. Mean Kendall-Tau correlations over BBOB functions with (≈100K) training data. Individual function results can be see in Appendix A.2.

In Table 4, as a sanity check over higher-dimensional functions, synthetic continuous objectives from the Black-box Optimization Benchmarking (BBOB) suite (Elhara et al., 2019) can also be sufficiently fitted by both the unnormalized and normalized decoder variants just as well as the pointwise and Riemann baselines.

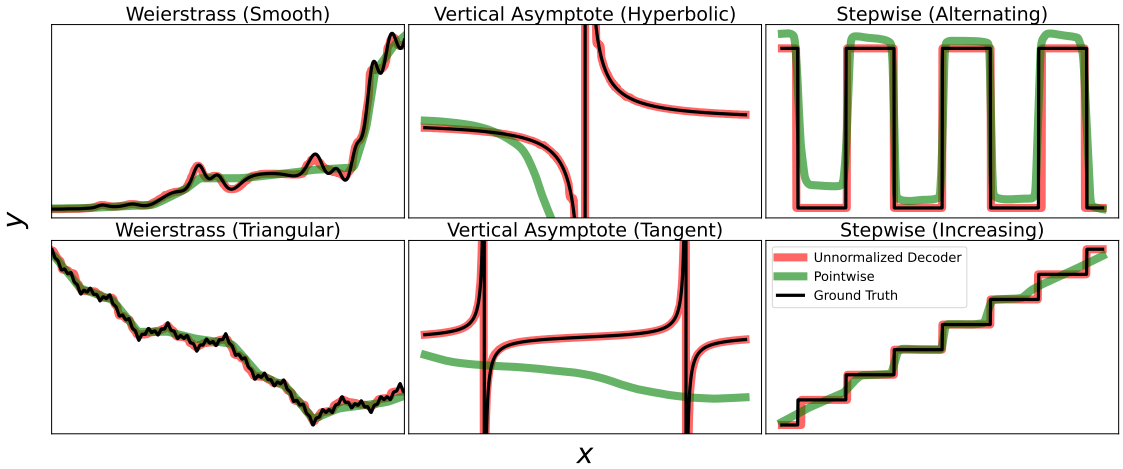

Figure 5: Fit to ground truth is better. Curve fitting plots for various 1D functions. Both models are trained over practically unlimited (x, y) points, where x is sampled from a bounded range.

4.2 Real-World Regression

In Figure 6 over real-world OpenML (Vanschoren et al., 2013) regression tasks from OpenML-CTR23 (Fischer et al., 2023) and AMLB (Gijsbers et al., 2024), we show that using the unnormalized decoder is competitive to using a regular pointwise head given the same amount of training data. In fact, we see that in the majority of tasks, the decoder outperforms the pointwise head, and in a few cases, the gap can be quite significant (>0.3).

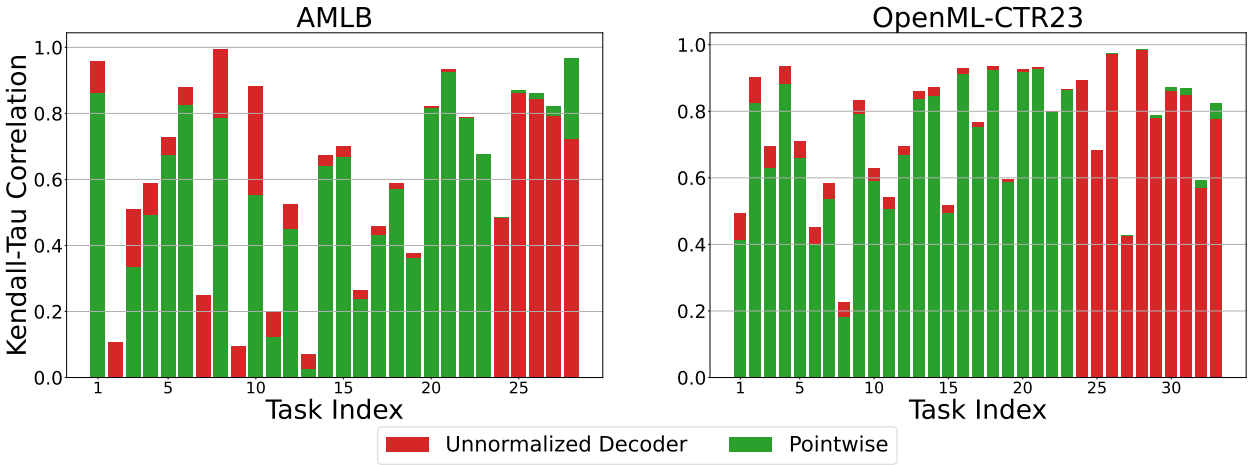

Figure 6: Higher (↑) is better. Kendall-Tau regression scores over AMLB and OpenML-CTR23 tasks using up to 10K maximum training points. Each bar averaged over 10 runs and bars from the same task (but different regressors) are stacked on top of each other and sorted by gap performance gap.

In Figure 7, we compare the use of a normalized decoder, Riemann histogram distribution head, and a pointwise head, when varying the amount of training data. We first observe the data inefficiency of using the histogram distribution on selected regression tasks - in certain cases, the histogram distribution plateaus, unable to even achieve the performance of decoding, regardless of the amount of training data.

Furthermore, interesting observations can be made when comparing against the standard pointwise baseline. In high data regimes ($\approx 10^4$ data points), there are cases in which it *also* plateaus earlier than the decoder. In low data regimes ($\approx 10^1$ data points), one would expect the decoder to struggle more as it needs to learn numeric token representations, but as it turns out, the pointwise head can perform worse due to numeric

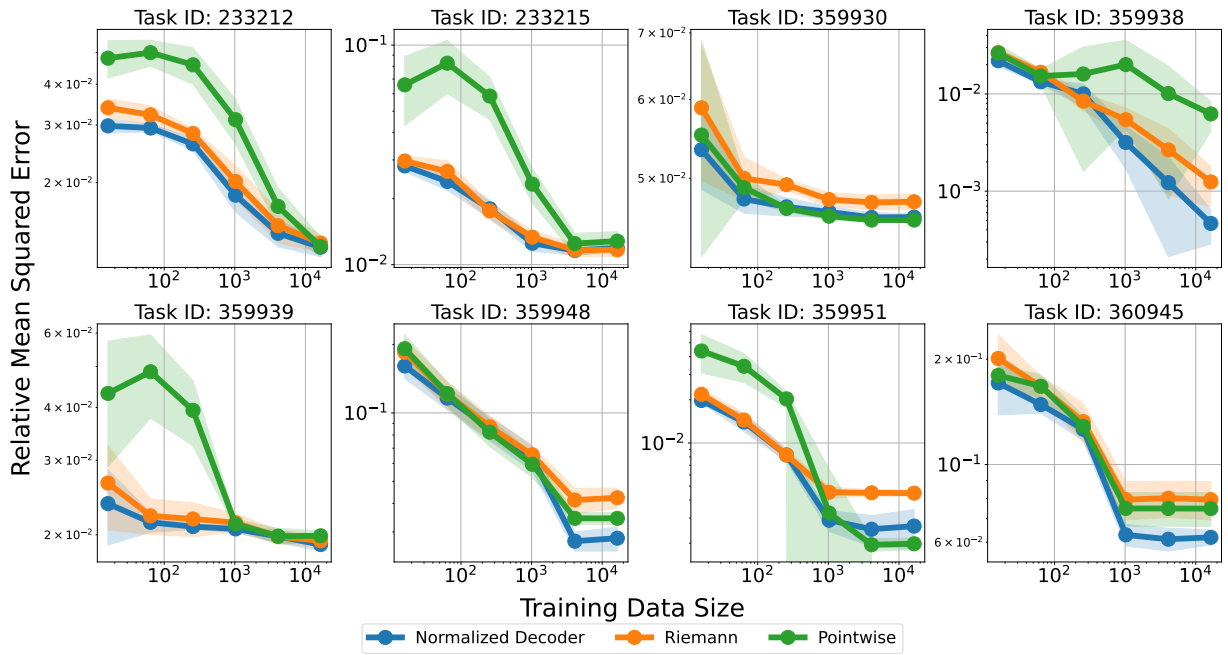

Figure 7: Lower (↓) is better. Relative mean squared error (MSE) over selected AMLB tasks. Each method used a min-max linear scaling normalization on y-values.

instabilities of its own. Due to undertraining, the pointwise head required appending a sigmoid activation to enforce the normalized output to be within [0,1] to avoid extremely high MSE errors.

4.3 Density Estimation

In Figure 8, we further see the decoder's ability to perform density estimation over various shapes. Given unbounded training data it is able to capture the overall distribution $p(y|x)$ well, although there can be slight outlier noise as shown by lighter points. In Appendix A.5 we show that even baselines such as Mixture Density Networks (MDNs) (Bishop, 1994) and Riemann distributions also suffer from this. While one can enforce the sampling to be tighter (e.g. lowering temperature) to remove noise, it can unfortunately also reduce expressivity. In general, we find that vanilla temperature sampling with temperature ≈1.0 is the best way to match $p(y|x)$.

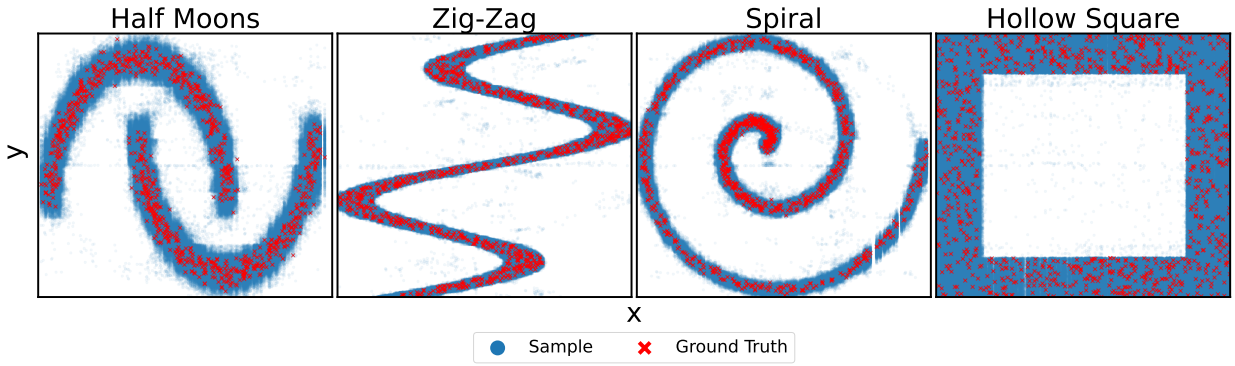

Figure 8: Fit to ground truth is better. Density estimation visualization over various shapes using an unnormalized decoder with vanilla temperature sampling.

In Table 1, we display the negative log-likelihood (NLL) on a collection of representative real-world datasets from the UCI regression repository (Dua & Graff, 2017) (full results over 25 datasets in Appendix A.4). We see that MDN performance has high variability, at times able to perform the best but also extremely poorly depending on the task. Meanwhile both decoding methods remain reliable overall (NLL<0.7 always). Interestingly, in comparison, the Riemann distribution consistently underperforms in every task.

Dataset	MDN	UD	ND	R
Airfoil	**0.12 ± 0.11**	0.40 ± 0.01	0.34 ± 0.01	1.33 ± 0.14
Bike	4.59 ± 0.86	0.12 ± 0.00	**0.10 ± 0.01**	0.36 ± 0.05
Elevators	0.30 ± 0.43	0.15 ± 0.00	**0.13 ± 0.00**	1.12 ± 0.02
Gas	0.68 ± 0.25	**0.02 ± 0.01**	**0.02 ± 0.00**	0.20 ± 0.09
Housing	**0.22 ± 0.13**	0.41 ± 0.03	0.38 ± 0.03	1.56 ± 0.21
Kin 40K	7.49 ± 0.73	0.19 ± 0.01	**0.12 ± 0.01**	0.39 ± 0.03
Pol	1.49 ± 0.41	**0.01 ± 0.00**	**0.01 ± 0.00**	0.18 ± 0.02
Protein	1.07 ± 0.44	**0.34 ± 0.00**	0.41 ± 0.01	1.55 ± 0.04
Pumadyn32nm	0.69 ± 1.26	**0.55 ± 0.00**	0.58 ± 0.02	2.32 ± 0.03
Wine	**0.05 ± 0.12**	0.24 ± 0.01	0.21 ± 0.01	1.67 ± 0.14
Yacht	**0.21 ± 0.10**	0.39 ± 0.02	0.23 ± 0.05	1.29 ± 0.38

Table 1: Lower (↓) is better. Avg. NLL (± StdDev) of test examples on UCI datasets over 10 train-test splits. Abbreviations: (UD, ND) = (unnormalized, normalized) decoders respectively; R = Riemann.

4.4 Ablation: Role of Decoder Size

We ablate the effect of the decoder size on performance. We first fix the tokenization for the normalized decoder (B=10, K=4) and then sweep the number of layers, heads, and hidden units. In Figure 9, we observe that larger decoder models do sometimes help, but only up to a certain point, at which overfitting can occur. This was also observed over regression over BBOB functions and with the unnormalized decoder, but we omitted these results for brevity.

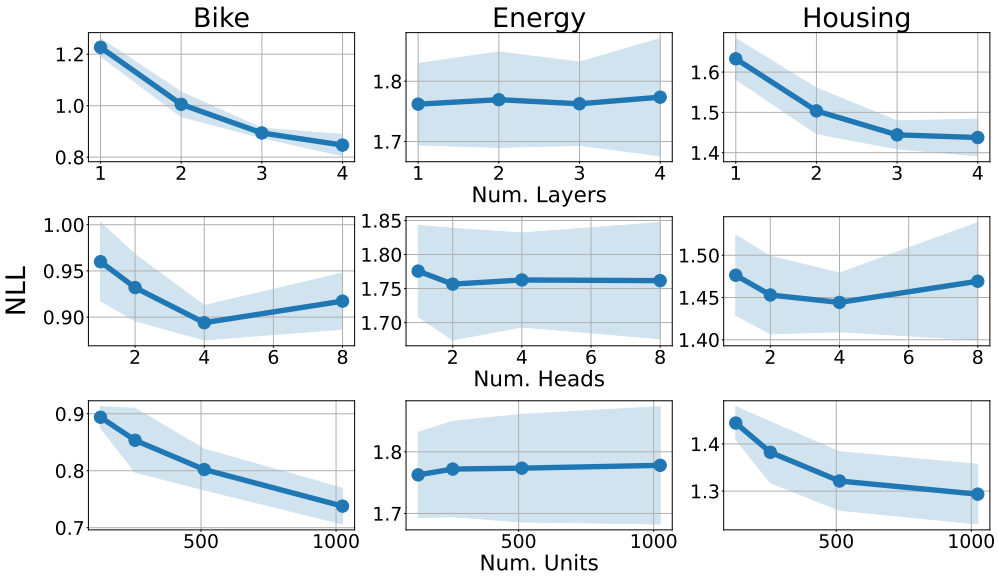

Figure 9: Lower (↓) is better. NLL over UCI datasets, when varying different axis (layers, heads, units) from a fixed default of (3, 4, 128) respectively.

4.5 Ablation: Error Correction

One can also improve regression behavior using techniques purely by modifying sequence representations. Inspired by the field of coding theory, we can use *error correction*, where we may simply have the decoder repeat its output multiple times $(t_1, \ldots, t_K, t'_1, \ldots, t'_K, t''_1, \ldots, t''_K, \ldots)$ during training, and at inference perform majority voting on each location $k \in \{1, \ldots, K\}$.

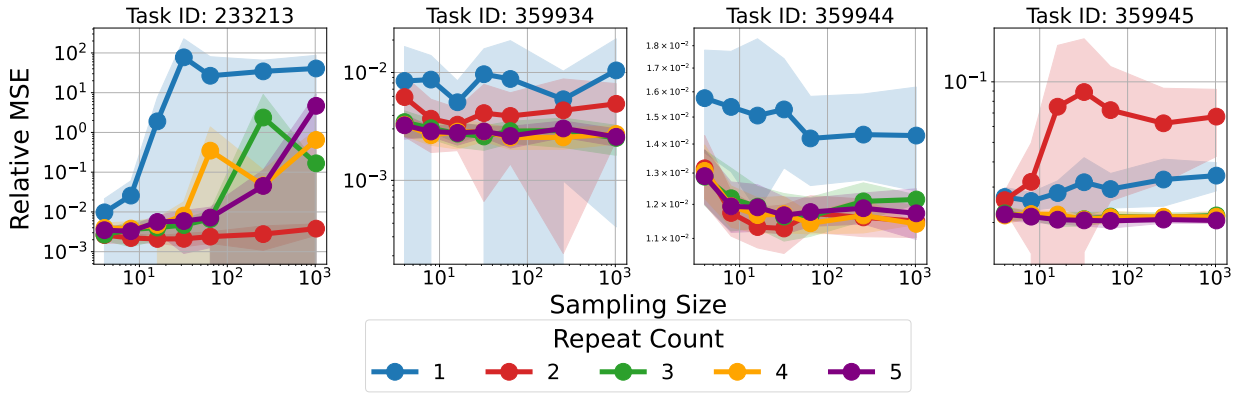

Figure 10: Lower (↓) is better. Relative MSE over selected AMLB tasks, when varying output repetitions.

In Figure 10, we focus on the unnormalized case when using mean aggregation, where performance can be significantly harmed from extreme outliers. We see that when using regular tokenization (repeat count=1), as more samples are drawn, the likelihood of drawing outliers increases the error. However, the error can be substantially decreased by training the model to repeat its output and allow better scaling with samples, although repeating too many times may make learning more difficult. Not all error correction techniques improve results however - in Appendix A.3, we briefly observe negative results applying other types of error correction, and we leave exploring the space of such methods for future work.

5 Impact Statement

This work establishes the validity of training using decoders on cross-entropy losses for regression. Regression is a broad method for many areas of machine learning and science, and there are multiple potential societal consequences for its application, none of which we feel must be specifically highlighted here.

6 Conclusion and Future Work

Throughout this paper, we thoroughly investigated the many benefits but also drawbacks of using decoding-based regression. We described a natural tokenization scheme for both normalized and unnormalized y-values, and theoretically established its risk minimization properties. Empirically, we showed that it can be competitive as, or even outperform traditional pointwise heads for regression tasks. Furthermore, it is also capable of density estimation over a variety of conditional distributions $p(y|x)$, and can further outperform common baselines such as Gaussian mixtures and Riemann distributions.

Numerous ways to extend decoding-based regression include improved tokenization schemes or other basis distributions besides piecewise constants. Further applications exist in other domains such as computer vision, where the encoder may be a convolutional network, or for multi-target regression, where the regressor needs to predict multiple different y-value targets. More broadly however, we hope this will also be a valuable reference for the language modeling community and that it provides a principled explanation for the use of supervised fine-tuning over numeric targets.

References

Yuntao Bai, Saurav Kadavath, Sandipan Kundu, Amanda Askell, Jackson Kernion, Andy Jones, Anna Chen, Anna Goldie, Azalia Mirhoseini, Cameron McKinnon, Carol Chen, Catherine Olsson, Christopher Olah, Danny Hernandez, Dawn Drain, Deep Ganguli, Dustin Li, Eli Tran-Johnson, Ethan Perez, Jamie Kerr, Jared Mueller, Jeffrey Ladish, Joshua Landau, Kamal Ndousse, Kamile Lukosiute, Liane Lovitt, Michael Sellitto, Nelson Elhage, Nicholas Schiefer, Noemí Mercado, Nova DasSarma, Robert Lasenby, Robin Larson, Sam Ringer, Scott Johnston, Shauna Kravec, Sheer El Showk, Stanislav Fort, Tamera Lanham, Timothy Telleen-Lawton, Tom Conerly, Tom Henighan, Tristan Hume, Samuel R. Bowman, Zac Hatfield-Dodds, Ben Mann, Dario Amodei, Nicholas Joseph, Sam McCandlish, Tom Brown, and Jared Kaplan. Constitutional AI: harmlessness from AI feedback. *CoRR*, abs/2212.08073, 2022. doi: 10.48550/ARXIV.2212.08073.

Marc G. Bellemare, Will Dabney, and Rémi Munos. A distributional perspective on reinforcement learning. In Doina Precup and Yee Whye Teh (eds.), *Proceedings of the 34th International Conference on Machine Learning, ICML 2017, Sydney, NSW, Australia, 6-11 August 2017*, volume 70 of *Proceedings of Machine Learning Research*, pp. 449–458. PMLR, 2017.

Christopher M. Bishop. Mixture density networks. Technical report, Aston University, 1994.

Ralph Allan Bradley and Milton E. Terry. Rank analysis of incomplete block designs: I. the method of paired comparisons. *Biometrika*, 39(3/4):324–345, 1952. ISSN 00063444, 14643510.

Wenzhi Cao, Vahid Mirjalili, and Sebastian Raschka. Rank consistent ordinal regression for neural networks with application to age estimation. *Pattern Recognit. Lett.*, 140:325–331, 2020. doi: 10.1016/J.PATREC.2020.11.008.

François Charton. Linear algebra with transformers. *Trans. Mach. Learn. Res.*, 2022, 2022.

Yutian Chen, Xingyou Song, Chansoo Lee, Zi Wang, Richard Zhang, David Dohan, Kazuya Kawakami, Greg Kochanski, Arnaud Doucet, Marc'Aurelio Ranzato, Sagi Perel, and Nando de Freitas. Towards learning universal hyperparameter optimizers with transformers. In Sanmi Koyejo, S. Mohamed, A. Agarwal, Danielle Belgrave, K. Cho, and A. Oh (eds.), *Advances in Neural Information Processing Systems 35: Annual Conference on Neural Information Processing Systems 2022, NeurIPS 2022, New Orleans, LA, USA, November 28 - December 9, 2022*, 2022.

Cheng-Han Chiang, Hung-yi Lee, and Michal Lukasik. TRACT: regression-aware fine-tuning meets chain-of-thought reasoning for llm-as-a-judge. *CoRR*, abs/2503.04381, 2025. doi: 10.48550/ARXIV.2503.04381.

Stéphane d'Ascoli, Pierre-Alexandre Kamienny, Guillaume Lample, and François Charton. Deep symbolic regression for recurrent sequences. *CoRR*, abs/2201.04600, 2022.

Raul Diaz and Amit Marathe. Soft labels for ordinal regression. In *IEEE Conference on Computer Vision and Pattern Recognition, CVPR 2019, Long Beach, CA, USA, June 16-20, 2019*, pp. 4738–4747. Computer Vision Foundation / IEEE, 2019. doi: 10.1109/CVPR.2019.00487.

Dheeru Dua and Casey Graff. UCI machine learning repository, 2017. URL `http://archive.ics.uci.edu/ml`.

Ouassim Elhara, Konstantinos Varelas, Duc Nguyen, Tea Tusar, Dimo Brockhoff, Nikolaus Hansen, and Anne Auger. Coco: the large scale black-box optimization benchmarking (bbob-largescale) test suite. *arXiv preprint arXiv:1903.06396*, 2019.

Angela Fan, Mike Lewis, and Yann N. Dauphin. Hierarchical neural story generation. In Iryna Gurevych and Yusuke Miyao (eds.), *Proceedings of the 56th Annual Meeting of the Association for Computational Linguistics, ACL 2018, Melbourne, Australia, July 15-20, 2018, Volume 1: Long Papers*, pp. 889–898. Association for Computational Linguistics, 2018. doi: 10.18653/V1/P18-1082.

Sebastian Felix Fischer, Liana Harutyunyan Matthias Feurer, and Bernd Bischl. OpenML-CTR23 – a curated tabular regression benchmarking suite. In *AutoML Conference 2023 (Workshop)*, 2023.

Pieter Gijsbers, Marcos L. P. Bueno, Stefan Coors, Erin LeDell, Sébastien Poirier, Janek Thomas, Bernd Bischl, and Joaquin Vanschoren. AMLB: an automl benchmark. *J. Mach. Learn. Res.*, 25:101:1–101:65, 2024.

Ethan Goan and Clinton Fookes. *Bayesian Neural Networks: An Introduction and Survey*. Springer International Publishing, Cham, 2020. ISBN 978-3-030-42553-1. doi: 10.1007/978-3-030-42553-1_3.

Alex Graves. Sequence transduction with recurrent neural networks. *CoRR*, abs/1211.3711, 2012.

Fredrik K. Gustafsson, Martin Danelljan, Goutam Bhat, and Thomas B. Schön. Energy-based models for deep probabilistic regression. In Andrea Vedaldi, Horst Bischof, Thomas Brox, and Jan-Michael Frahm (eds.), *Computer Vision - ECCV 2020 - 16th European Conference, Glasgow, UK, August 23-28, 2020, Proceedings, Part XX*, volume 12365 of *Lecture Notes in Computer Science*, pp. 325–343. Springer, 2020. doi: 10.1007/978-3-030-58565-5_20.

Frank E. Harrell and C. E. Davis. A new distribution-free quantile estimator. *Biometrika*, 69(3):635–640, 1982. ISSN 00063444, 14643510.

Noah Hollmann, Samuel Müller, Lennart Purucker, Arjun Krishnakumar, Max Körfer, Shi Bin Hoo, Robin Tibor Schirrmeister, and Frank Hutter. Accurate predictions on small data with a tabular foundation model. *Nat.*, 637(8044):319–326, 2025. doi: 10.1038/S41586-024-08328-6.

Ari Holtzman, Jan Buys, Li Du, Maxwell Forbes, and Yejin Choi. The curious case of neural text degeneration. In *8th International Conference on Learning Representations, ICLR 2020, Addis Ababa, Ethiopia, April 26-30, 2020*. OpenReview.net, 2020.

IEEE. Ieee standard for floating-point arithmetic. *IEEE Std 754-2019 (Revision of IEEE 754-2008)*, pp. 1–84, 2019. doi: 10.1109/IEEESTD.2019.8766229.

Ehsan Imani and Martha White. Improving regression performance with distributional losses. In Jennifer G. Dy and Andreas Krause (eds.), *Proceedings of the 35th International Conference on Machine Learning, ICML 2018, Stockholmsmässan, Stockholm, Sweden, July 10-15, 2018*, volume 80 of *Proceedings of Machine Learning Research*, pp. 2162–2171. PMLR, 2018.

Jouko Lampinen and Aki Vehtari. Bayesian approach for neural networks–review and case studies. *Neural Networks*, 14(3):257–274, 2001. doi: 10.1016/S0893-6080(00)00098-8.

L.E. Lehmann. *Theory of Point Estimation*. A Wiley publication in mathematical statistics. Wiley, 1983.

Xixi Liu, Che-Tsung Lin, and Christopher Zach. Energy-based models for deep probabilistic regression. In *2022 26th International Conference on Pattern Recognition (ICPR)*, pp. 2693–2699, 2022. doi: 10.1109/ICPR56361.2022.9955636.

Michal Lukasik, Harikrishna Narasimhan, Aditya Krishna Menon, Felix Yu, and Sanjiv Kumar. Regression aware inference with llms. In Yaser Al-Onaizan, Mohit Bansal, and Yun-Nung Chen (eds.), *Findings of the Association for Computational Linguistics: EMNLP 2024, Miami, Florida, USA, November 12-16, 2024*, pp. 13667–13678. Association for Computational Linguistics, 2024.

Michal Lukasik, Zhao Meng, Harikrishna Narasimhan, Aditya Krishna Menon, Yin Wen Chang, Felix X. Yu, and Sanjiv Kumar. Better autoregressive regression with LLMs. In *The Thirteenth International Conference on Learning Representations, ICLR 2025, Singapore, Singapore, April 24-28, 2025*. OpenReview.net, 2025.

Dakota Mahan, Duy Phung, Rafael Rafailov, Chase Blagden, Nathan Lile, Louis Castricato, Jan-Philipp Fränken, Chelsea Finn, and Alon Albalak. Generative reward models. *CoRR*, abs/2410.12832, 2024. doi: 10.48550/ARXIV.2410.12832.

Radford M. Neal. Connectionist learning of belief networks. *Artif. Intell.*, 56(1):71–113, 1992. doi: 10.1016/0004-3702(92)90065-6.

Tung Nguyen, Qiuyi Zhang, Bangding Yang, Chansoo Lee, Jorg Bornschein, Yingjie Miao, Sagi Perel, Yutian Chen, and Xingyou Song. Predicting from strings: Language model embeddings for bayesian optimization. *CoRR*, abs/2410.10190, 2024. doi: 10.48550/ARXIV.2410.10190.

Rodrigo Frassetto Nogueira, Zhiying Jiang, and Jimmy Lin. Investigating the limitations of the transformers with simple arithmetic tasks. *CoRR*, abs/2102.13019, 2021.

Emanuel Parzen. On Estimation of a Probability Density Function and Mode. *The Annals of Mathematical Statistics*, 33(3):1065 – 1076, 1962. doi: 10.1214/aoms/1177704472.

Minghai Qin. Hamming-distance-based binary representation of numbers. In *2018 IEEE International Symposium on Information Theory (ISIT)*, pp. 2202–2205, 2018. doi: 10.1109/ISIT.2018.8437644.

Carl Edward Rasmussen. The infinite gaussian mixture model. In Sara A. Solla, Todd K. Leen, and Klaus-Robert Müller (eds.), *Advances in Neural Information Processing Systems 12, [NIPS Conference, Denver, Colorado, USA, November 29 - December 4, 1999]*, pp. 554–560. The MIT Press, 1999.

Murray Rosenblatt. Remarks on Some Nonparametric Estimates of a Density Function. *The Annals of Mathematical Statistics*, 27(3):832 – 837, 1956. doi: 10.1214/aoms/1177728190.

Xingyou Song, Oscar Li, Chansoo Lee, Bangding Yang, Daiyi Peng, Sagi Perel, and Yutian Chen. Omnipred: Language models as universal regressors. *CoRR*, abs/2402.14547, 2024.

Eric Tang, Bangding Yang, and Xingyou Song. Understanding LLM embeddings for regression. *CoRR*, abs/2411.14708, 2024. doi: 10.48550/ARXIV.2411.14708.

Yichuan Tang and Ruslan Salakhutdinov. Learning stochastic feedforward neural networks. In Christopher J. C. Burges, Léon Bottou, Zoubin Ghahramani, and Kilian Q. Weinberger (eds.), *Advances in Neural Information Processing Systems 26: 27th Annual Conference on Neural Information Processing Systems 2013. Proceedings of a meeting held December 5-8, 2013, Lake Tahoe, Nevada, United States*, pp. 530–538, 2013.

Yee Whye Teh, Max Welling, Simon Osindero, and Geoffrey E. Hinton. Energy-based models for sparse overcomplete representations. *J. Mach. Learn. Res.*, 4:1235–1260, 2003.

D. M. Titterington. Bayesian Methods for Neural Networks and Related Models. *Statistical Science*, 19(1): 128 – 139, 2004. doi: 10.1214/088342304000000099.

Robert Vacareanu, Vlad-Andrei Negru, Vasile Suciu, and Mihai Surdeanu. From words to numbers: Your large language model is secretly A capable regressor when given in-context examples. *CoRR*, abs/2404.07544, 2024.

Joaquin Vanschoren, Jan N. van Rijn, Bernd Bischl, and Luís Torgo. Openml: networked science in machine learning. *SIGKDD Explor.*, 15(2):49–60, 2013. doi: 10.1145/2641190.2641198.

Ashish Vaswani, Noam Shazeer, Niki Parmar, Jakob Uszkoreit, Llion Jones, Aidan N. Gomez, Lukasz Kaiser, and Illia Polosukhin. Attention is all you need. In Isabelle Guyon, Ulrike von Luxburg, Samy Bengio, Hanna M. Wallach, Rob Fergus, S. V. N. Vishwanathan, and Roman Garnett (eds.), *Advances in Neural Information Processing Systems 30: Annual Conference on Neural Information Processing Systems 2017, December 4-9, 2017, Long Beach, CA, USA*, pp. 5998–6008, 2017.

Marek Wydmuch, Kalina Jasinska, Mikhail Kuznetsov, Róbert Busa-Fekete, and Krzysztof Dembczynski. A no-regret generalization of hierarchical softmax to extreme multi-label classification. In Samy Bengio, Hanna M. Wallach, Hugo Larochelle, Kristen Grauman, Nicolò Cesa-Bianchi, and Roman Garnett (eds.), *Advances in Neural Information Processing Systems 31: Annual Conference on Neural Information Processing Systems 2018, NeurIPS 2018, December 3-8, 2018, Montréal, Canada*, pp. 6358–6368, 2018.

Lunjun Zhang, Arian Hosseini, Hritik Bansal, Mehran Kazemi, Aviral Kumar, and Rishabh Agarwal. Generative verifiers: Reward modeling as next-token prediction. *CoRR*, abs/2408.15240, 2024. doi: 10.48550/ARXIV.2408.15240.

Lianmin Zheng, Wei-Lin Chiang, Ying Sheng, Siyuan Zhuang, Zhanghao Wu, Yonghao Zhuang, Zi Lin, Zhuohan Li, Dacheng Li, Eric P. Xing, Hao Zhang, Joseph E. Gonzalez, and Ion Stoica. Judging llm-as-a-judge with mt-bench and chatbot arena. In *Advances in Neural Information Processing Systems 36: Annual Conference on Neural Information Processing Systems 2023, NeurIPS 2023, New Orleans, LA, USA, December 10 - 16, 2023*, 2023.

Daniel M. Ziegler, Nisan Stiennon, Jeffrey Wu, Tom B. Brown, Alec Radford, Dario Amodei, Paul F. Christiano, and Geoffrey Irving. Fine-tuning language models from human preferences. *CoRR*, abs/1909.08593, 2019.

Appendix

A Additional Experiments

A.1 Data Scaling: Extended

For completeness, we display the plots over all tasks in AMLB (Gijsbers et al., 2024). We confirm the data-efficiency of the decoder head against the Riemann distribution head on nearly every regression task. Furthermore, we observe numerous cases where both distributional methods outperform the pointwise head, especially in low data regimes.

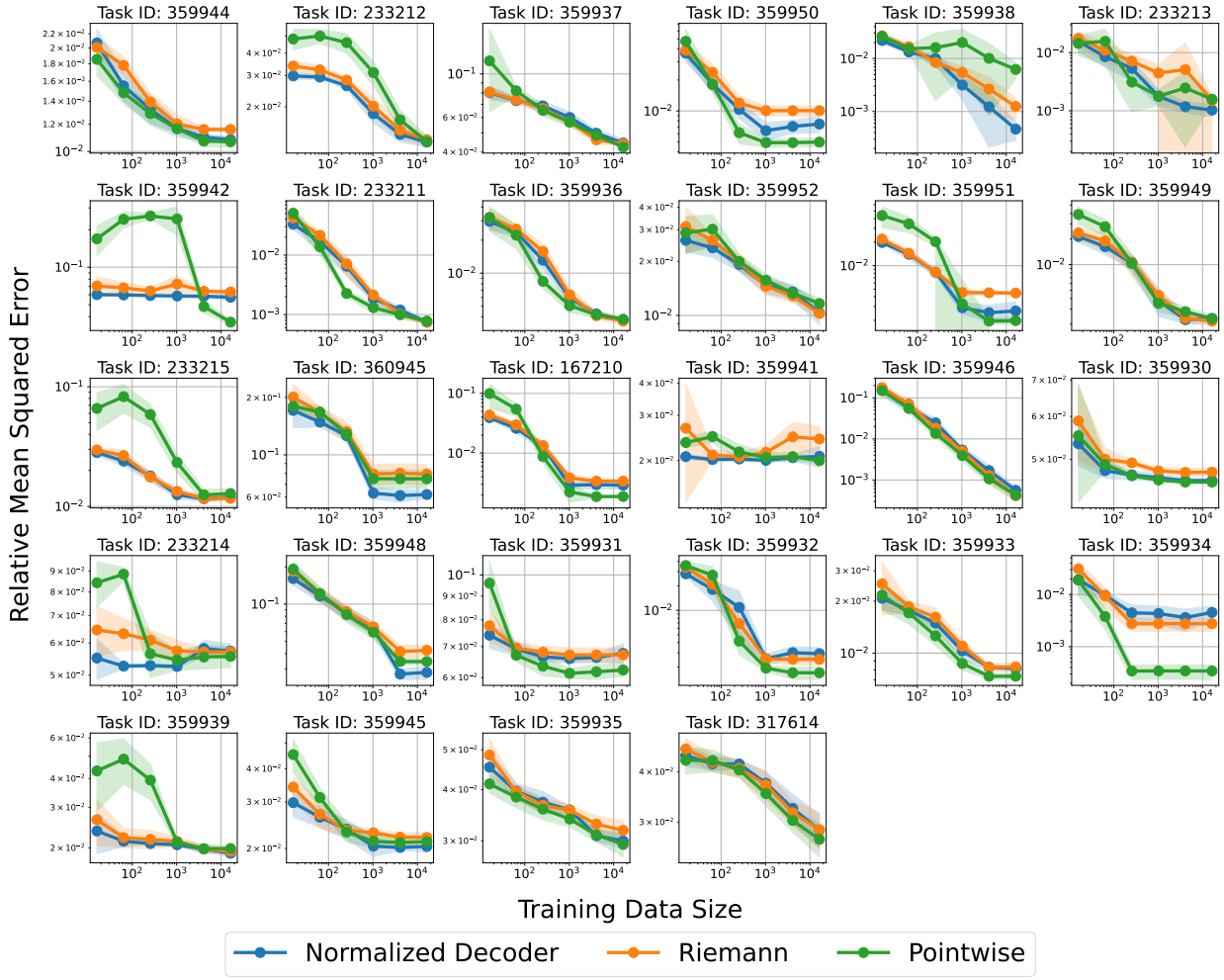

Figure 11: Lower (↓) is better. Regression performance as a function of training data scaling between using the normalized decoder vs. Reimannian distribution as regression heads. Each point was averaged over 10 training runs over random combinations of datapoints from the original AMLB task's training set.

A.2 BBOB Curve Fitting: Extended

In Figure 12, we compare the curve fitting properties of multiple regression heads. We see overall that the decoder head is competitive and has both pros and cons for specific function landscapes from the BBOB benchmark.

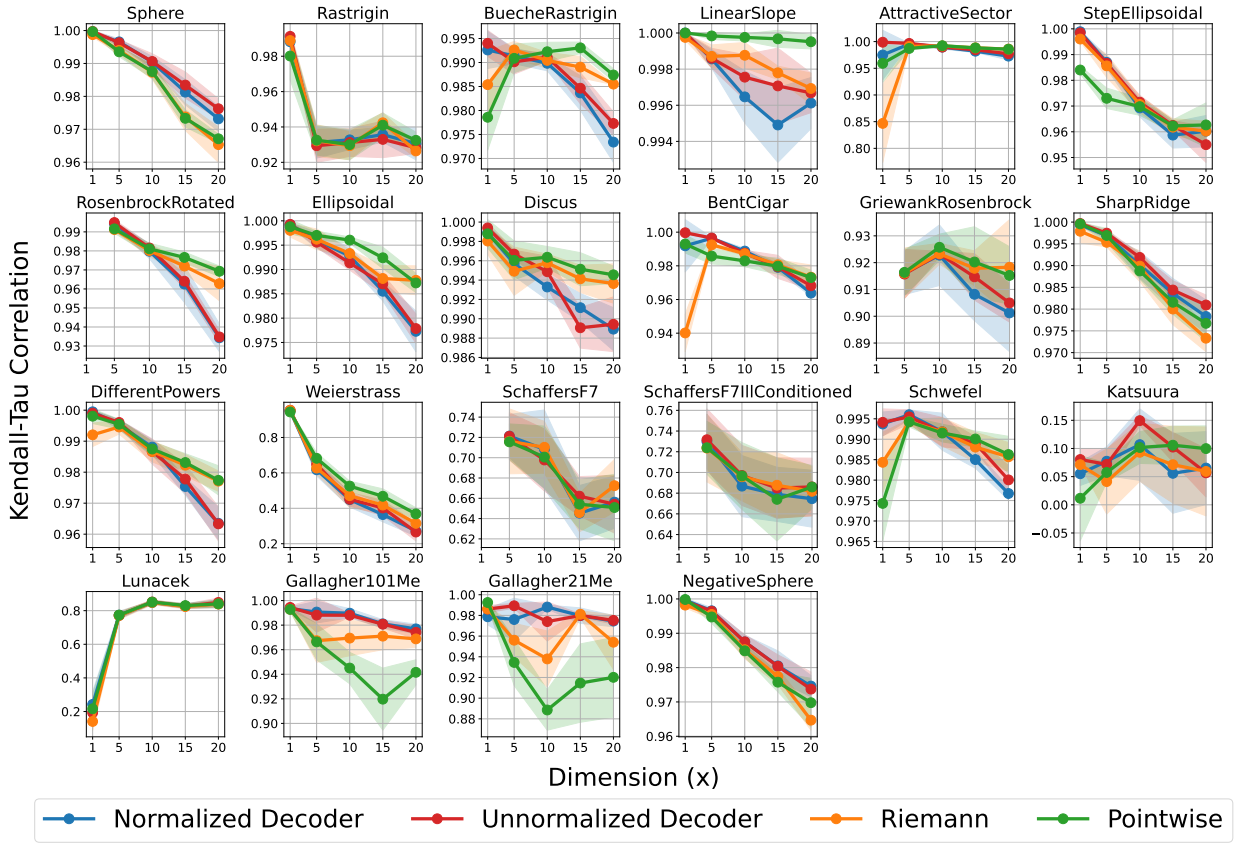

Figure 12: Higher (↑) is better. Extended results from Table 4 in the main body. Regression performance as a function of input dimension over BBOB functions using Kendall-Tau correlation. Each point was averaged over 10 training runs, each with 100K training points (x, y) where each x is sampled uniformly from $[-5, 5]$ coordinate-wise. **Note:** Some functions such as RosenbrockRotated or GriewankRosenbrock are undefined when dimension is 1, so we skip those points.

A.3 Alternative Tokenization Schemes: Hamming-Distance

One possible criticism of the default tree-based tokenization in the normalized decoding case, is the vulnerability to small changes in the left-most significant tokens, which can cause large numeric changes in the actual number. Qin (2018) notes this and proposes an alternative "Hamming Distance-based" binary representation which is robust to bitwise edits, and upper bounds the possible distortion $|y' - y|$ as a function of the edit distance between the Hamming representations of y' and y. For example, if the binary length is 3, the representation for all integers $\{0, 1, \ldots, 2^3\}$ is $\{(000), (001), (010), (100), (011), (101), (110), (111)\}$ which can also be used in the normalized case for $\{0/2^3, 1/2^3, \ldots, 7/2^3\} \subset [0, 1]$. In Figure 13, we show however, such a representation may *not* lead to better regression results, which we hypothesize is due to this representation being more difficult to learn.

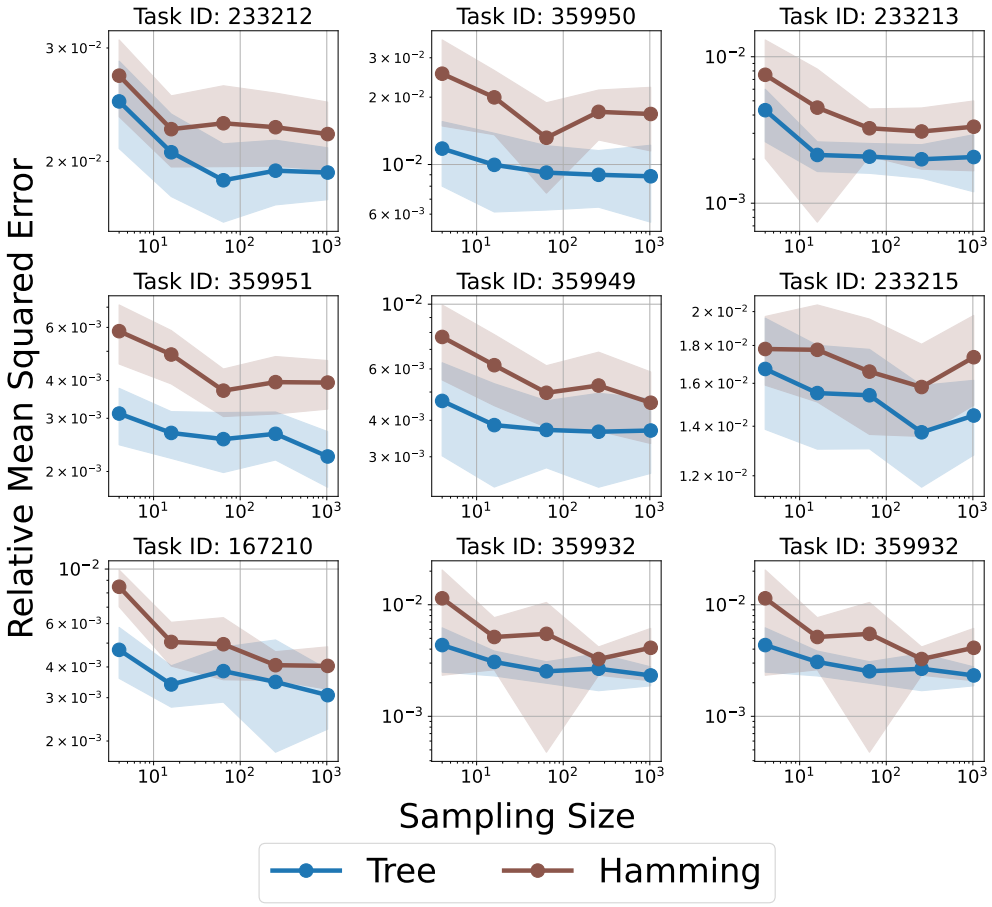

Figure 13: Lower (↓) is better. Regression performance while vary sampling size from $y \sim p_\theta(\cdot|x)$ using binary tree-based tokenization vs. Hamming representation on normalized decoder with mean aggregation. Each point was averaged over 10 training runs over random size-1000 combinations of the original AMLB task's training data points.

A.4 Full UCI Density Estimation Results

We obtained the datasets from `https://github.com/treforevans/uci_datasets` which preprocessed and scraped the data from the official UCI website at `https://archive.ics.uci.edu/`.

Dataset	Mixture Density Network	Unnormalized Decoder	Normalized Decoder	Riemann
Airfoil	**0.12 ± 0.11**	0.40 ± 0.01	0.34 ± 0.01	1.33 ± 0.14
AutoMPG	**0.21 ± 0.07**	0.32 ± 0.03	0.41 ± 0.05	1.62 ± 0.17
Autos	**0.32 ± 0.23**	0.48 ± 0.05	0.47 ± 0.07	2.60 ± 0.76
Bike	4.59 ± 0.86	0.12 ± 0.00	**0.10 ± 0.01**	0.36 ± 0.05
BreastCancer	**0.32 ± 0.09**	0.48 ± 0.05	0.64 ± 0.03	2.85 ± 0.37
Challenger	**-0.29 ± 0.66**	0.14 ± 0.14	0.06 ± 0.08	0.87 ± 0.77
Concrete	**0.15 ± 0.05**	0.43 ± 0.03	0.41 ± 0.04	1.67 ± 0.20
Elevators	0.30 ± 0.43	0.15 ± 0.00	**0.13 ± 0.00**	1.12 ± 0.02
Energy	0.40 ± 0.14	0.17 ± 0.03	**0.16 ± 0.05**	0.38 ± 0.20
Fertility	**-0.06 ± 0.16**	0.31 ± 0.09	0.46 ± 0.13	2.41 ± 0.61
Gas	0.68 ± 0.25	**0.02 ± 0.01**	**0.02 ± 0.00**	0.20 ± 0.09
Housing	**0.22 ± 0.13**	0.41 ± 0.03	0.38 ± 0.03	1.56 ± 0.21
KeggDirected	2.41 ± 1.10	**0.05 ± 0.00**	**0.05 ± 0.00**	0.22 ± 0.02
Kin 40K	7.49 ± 0.73	0.19 ± 0.01	**0.12 ± 0.01**	0.39 ± 0.03
Parkinsons	0.59 ± 0.18	0.40 ± 0.02	**0.39 ± 0.03**	1.40 ± 0.33
Pol	1.49 ± 0.41	**0.01 ± 0.00**	**0.01 ± 0.00**	0.18 ± 0.02
Protein	1.07 ± 0.44	**0.34 ± 0.00**	0.41 ± 0.01	1.55 ± 0.04
Pumadyn32nm	0.69 ± 1.26	**0.55 ± 0.00**	0.58 ± 0.02	2.32 ± 0.03
Slice	7.09 ± 0.09	0.05 ± 0.00	**0.02 ± 0.00**	0.08 ± 0.02
SML	1.31 ± 0.59	0.21 ± 0.01	**0.11 ± 0.01**	0.35 ± 0.03
Solar	**-1.40 ± 0.29**	0.04 ± 0.01	0.04 ± 0.01	0.61 ± 0.12
Stock	**-0.15 ± 0.15**	0.27 ± 0.04	0.32 ± 0.04	1.63 ± 0.46
TamiElectric	**0.01 ± 0.00**	0.46 ± 0.00	0.69 ± 0.00	2.70 ± 0.00
Wine	**0.05 ± 0.12**	0.24 ± 0.01	0.21 ± 0.01	1.67 ± 0.14
Yacht	**0.21 ± 0.10**	0.39 ± 0.02	0.23 ± 0.05	1.29 ± 0.38

Table 2: Lower (↓) is better. Avg. NLL (± StdDev) of test examples on UCI datasets over 10 train-test splits.

A.5 Density Estimation Visualization: Extended

In Figure 14, we present further results on density estimation with various decoder sampling techniques (top-k, top-p, low temperature) alongside MDN and Riemann baselines. We see that using vanilla temperature sampling for the decoder is optimal and unbiased for capturing the shapes of all problems.

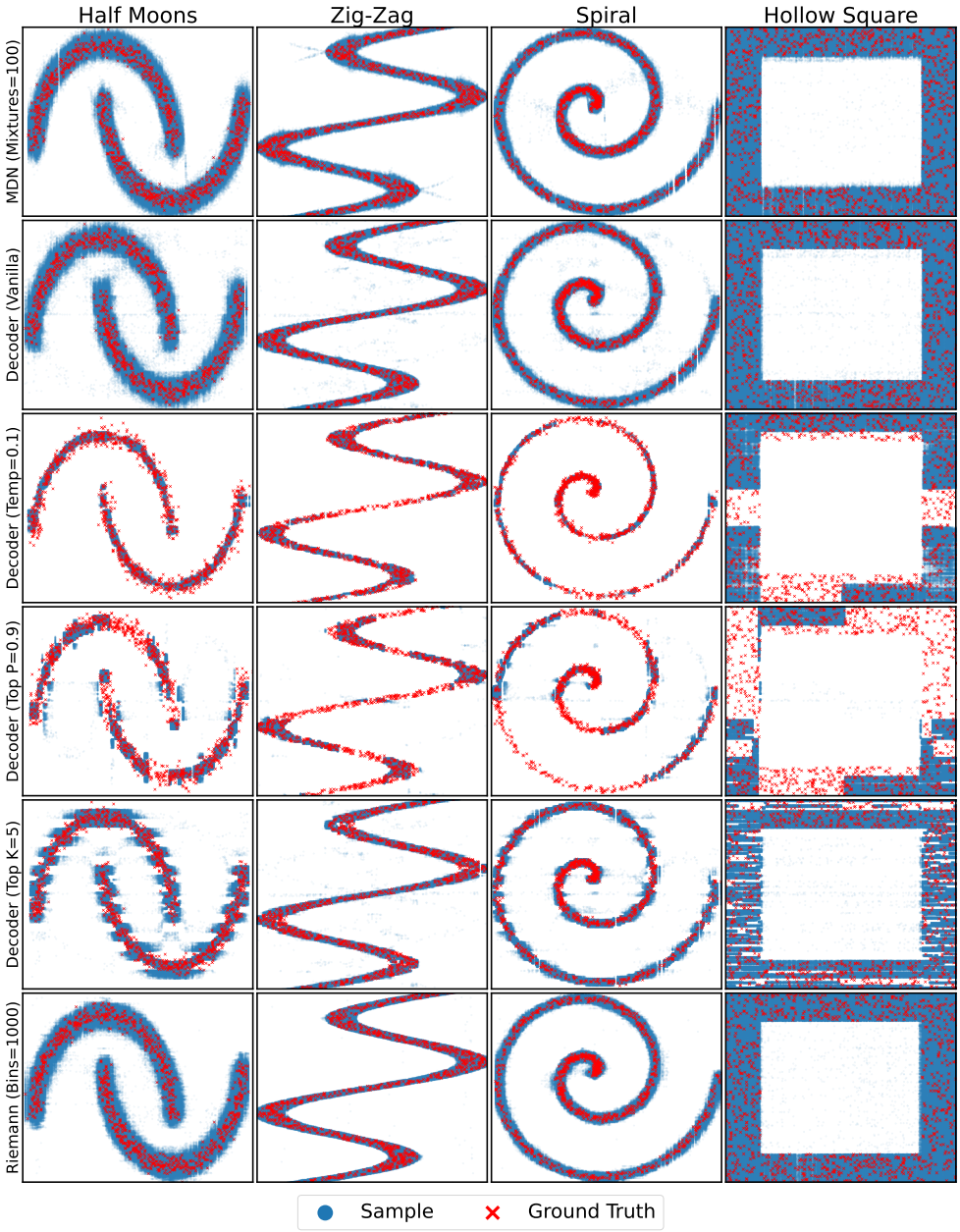

Figure 14: Visualizing density estimation of $p(y|x)$ on 1D problems. We used an unnormalized decoder with $(B = 10, E = 1, M = 5)$.

B Extended Theory

Proof of Theorem 1. Firstly, we observe that

$$\operatorname*{argmin}_{\theta} \frac{1}{N} \sum_{n=1}^{N} -\log p_\theta(\lambda_K(Y_n)) = \operatorname*{argmin}_{\theta} H(\widetilde{f}_N^K, p_\theta),$$

where $\widetilde{f}_N^k$ is a discrete distribution that tracks the fraction of samples $\{Y_n\}_{n=1}^N$ that fall within each of the 2^k uniformly-spaced bins in $[0,1]$. Formally,

$$\widetilde{f}_N^k((b_1,\ldots,b_k)) = \frac{1}{N}\sum_{n=1}^{N} \mathbf{1}(\lambda_k(Y_n) = (b_1,\ldots,b_k)).$$

Conditioned on the samples $\{Y_n\}_{n=1}^N$, $\widetilde{f}_N^k$ is a distribution on k-bit strings, and so by the K-bit universality assumption, $p_{\theta^*}^K = \widetilde{f}_N^K$. It follows that $p_{\theta^*}^k = \widetilde{f}_N^k$ $\forall k \leq K$ since if two discrete distributions are equal so are any of their marginals. Then $f_N^{k*}(x) \equiv 2^k p_{\theta^*}^k(\lambda_k(x)) = 2^k \widetilde{f}_N^k(\lambda_k(x))$ lines up exactly as a 2^k-bin histogram estimator for f, for all $k \leq K$.

Now, we can treat the problem as one of histogram estimation. Let's consider a fixed k. We first observe that the risk can be written as the sum of a squared bias term and a variance one. Specifically,

$$R(f, f_N^{k*}) = \int_0^1 \text{Bias}(y)^2 dy + \int_0^1 \text{Variance}(y) dy,$$

where $\text{Bias}(y) = \mathbb{E}[f_N^{k*}(y)] - f(y)$ and $\text{Variance}(y) = \mathbb{V}(f_N^{k*}(y))$ is the bias and variance of $f_N^{k*}(y)$ at fixed y respectively.

Now, label bins $\{B_j\}_{j=0}^{2^k-1}$, where $B_j = [j\varepsilon, (j+1)\varepsilon)$ and $\varepsilon = 2^{-k}$ is the bin width. Let $p_j = \int_{B_j} f(z)dz$ be the true probability mass in bin B_j. With N_j as the number of samples in B_j, the expected value of the estimator for $y \in B_j$ is $\mathbb{E}[f_N^{k*}(y)] = \mathbb{E}[N_j/(N\varepsilon)] = (Np_j)/(N\varepsilon) = p_j/\varepsilon$.

Assume the true density f is twice continuously differentiable on $[0,1]$ (i.e., $f \in C^2([0,1])$). This implies f, f', and f'' are bounded on $[0,1]$. Let $M_1 = \sup_{y\in[0,1]} |f'(y)|$ and $M_2 = \sup_{y\in[0,1]} |f''(y)|$.

Bias Analysis: Let $y_j = (j+1/2)\varepsilon$ be the midpoint of bin B_j. For $z \in B_j$, by Taylor's Theorem around y_j: $f(z) = f(y_j) + (z-y_j)f'(y_j) + \frac{(z-y_j)^2}{2} f''(\xi_z)$ for some ξ_z between z and y_j. Integrating over B_j:

$$\begin{aligned} p_j = \int_{B_j} f(z)dz &= \int_{B_j} \left[f(y_j) + (z-y_j)f'(y_j) + \frac{(z-y_j)^2}{2} f''(\xi_z) \right] dz \\ &= f(y_j)\int_{B_j} dz + f'(y_j)\int_{B_j} (z-y_j)dz + \int_{B_j} \frac{(z-y_j)^2}{2} f''(\xi_z)dz \\ &= \varepsilon f(y_j) + 0 + R_j, \end{aligned}$$

where the remainder term $R_j = \int_{B_j} \frac{(z-y_j)^2}{2} f''(\xi_z)dz$. Since $|z-y_j| \leq \varepsilon/2$ and $|f''(\xi_z)| \leq M_2$, we have $|R_j| \leq \int_{B_j} \frac{(\varepsilon/2)^2}{2} M_2 dz = \frac{M_2\varepsilon^2}{8}\int_{B_j} dz = \frac{M_2\varepsilon^3}{8}$. Thus, $R_j = \mathcal{O}(\varepsilon^3)$.

The bias for $y \in B_j$ is $\text{Bias}(y) = \mathbb{E}[f_N^{k*}(y)] - f(y) = \frac{p_j}{\varepsilon} - f(y) = \frac{\varepsilon f(y_j) + R_j}{\varepsilon} - f(y) = f(y_j) + \frac{R_j}{\varepsilon} - f(y)$. Expanding $f(y)$ around y_j: $f(y) = f(y_j) + (y-y_j)f'(y_j) + \frac{(y-y_j)^2}{2} f''(\eta_y)$ for η_y between y and y_j.

$$\begin{aligned} \text{Bias}(y) &= f(y_j) + \mathcal{O}(\varepsilon^2) - \left[f(y_j) + (y-y_j)f'(y_j) + \mathcal{O}(\varepsilon^2) \right] \\ &= -(y-y_j)f'(y_j) + \mathcal{O}(\varepsilon^2). \end{aligned}$$

Now, integrate the squared bias over bin B_j:

$$\begin{aligned}
\int_{B_j} \text{Bias}(y)^2 dy &= \int_{B_j} \left[-(y-y_j)f'(y_j) + \mathcal{O}(\varepsilon^2)\right]^2 dy \\
&= \int_{B_j} \left[(y-y_j)^2 (f'(y_j))^2 - 2(y-y_j)f'(y_j)\mathcal{O}(\varepsilon^2) + \mathcal{O}(\varepsilon^4)\right] dy \\
&= (f'(y_j))^2 \int_{B_j} (y-y_j)^2 dy - \mathcal{O}(\varepsilon^2) f'(y_j) \int_{B_j} (y-y_j) dy + \int_{B_j} \mathcal{O}(\varepsilon^4) dy \\
&= (f'(y_j))^2 \int_{-\varepsilon/2}^{\varepsilon/2} u^2 du - \mathcal{O}(\varepsilon^2) f'(y_j) \cdot 0 + \mathcal{O}(\varepsilon^4) \cdot \varepsilon \quad (\text{let } u = y - y_j) \\
&= (f'(y_j))^2 \left[\frac{u^3}{3}\right]_{-\varepsilon/2}^{\varepsilon/2} + \mathcal{O}(\varepsilon^5) \\
&= (f'(y_j))^2 \frac{\varepsilon^3}{12} + \mathcal{O}(\varepsilon^5).
\end{aligned}$$

Summing over all bins:

$$\begin{aligned}
\int_0^1 \text{Bias}(y)^2 dy = \sum_{j=0}^{2^k-1} \int_{B_j} \text{Bias}(y)^2 dy &= \sum_{j=0}^{2^k-1} \left[(f'(y_j))^2 \frac{\varepsilon^3}{12} + \mathcal{O}(\varepsilon^5)\right] \\
&= \frac{\varepsilon^2}{12} \sum_{j=0}^{2^k-1} (f'(y_j))^2 \varepsilon + \sum_{j=0}^{2^k-1} \mathcal{O}(\varepsilon^5) \\
&= \frac{\varepsilon^2}{12} \left(\int_0^1 (f'(y))^2 dy + \mathcal{O}(\varepsilon^2)\right) + 2^k \mathcal{O}(\varepsilon^5) \\
&= \frac{\varepsilon^2}{12} \int_0^1 (f'(y))^2 dy + \mathcal{O}(\varepsilon^4),
\end{aligned}$$

where the third line uses a known approximation error for the Riemann sum with midpoint rule applied to $(f')^2 \in C^1$.

Variance Analysis: The variance for $y \in B_j$ is $\text{Variance}(y) = \mathbb{V}(f_N^{k*}(y)) = \mathbb{V}(N_j/(N\varepsilon)) = \frac{1}{(N\varepsilon)^2}\mathbb{V}(N_j)$. Since $N_j \sim \text{Binomial}(N, p_j)$, $\mathbb{V}(N_j) = Np_j(1-p_j)$.

$$\begin{aligned}
\text{Variance}(y) &= \frac{Np_j(1-p_j)}{N^2\varepsilon^2} = \frac{p_j(1-p_j)}{N\varepsilon^2} \\
&= \frac{(\varepsilon f(y_j) + \mathcal{O}(\varepsilon^3))(1 - \varepsilon f(y_j) - \mathcal{O}(\varepsilon^3))}{N\varepsilon^2} \\
&= \frac{\varepsilon f(y_j) - \varepsilon^2 f(y_j)^2 + \mathcal{O}(\varepsilon^3)}{N\varepsilon^2} \\
&= \frac{f(y_j)}{N\varepsilon} - \frac{f(y_j)^2}{N} + \mathcal{O}(\varepsilon/N).
\end{aligned}$$

Integrating the variance:

$$\begin{aligned}
\int_0^1 \text{Variance}(y)dy &= \sum_{j=0}^{2^k-1} \int_{B_j} \left(\frac{f(y_j)}{N\varepsilon} + \mathcal{O}(1/N) \right) dy \\
&= \sum_{j=0}^{2^k-1} \left(\frac{f(y_j)\varepsilon}{N\varepsilon} + \mathcal{O}(\varepsilon/N) \right) \\
&= \frac{1}{N\varepsilon} \sum_{j=0}^{2^k-1} f(y_j)\varepsilon + 2^k \mathcal{O}(\varepsilon/N) \\
&= \frac{1}{N\varepsilon} \left(\int_0^1 f(y)dy + \mathcal{O}(\varepsilon^2) \right) + \mathcal{O}(1/N) \quad \text{(Riemann sum error for } f \in C^2) \\
&= \frac{1}{N\varepsilon}(1 + \mathcal{O}(\varepsilon^2)) + \mathcal{O}(1/N) \\
&= \frac{1}{N\varepsilon} + \mathcal{O}(\varepsilon/N) + \mathcal{O}(1/N).
\end{aligned}$$

Since we typically consider asymptotics where $N \to \infty$ and $\varepsilon \to 0$ such that $N\varepsilon \to \infty$, the dominant variance term is $1/(N\varepsilon)$.

Total Risk: Combining the integrated squared bias and integrated variance:

$$\begin{aligned}
R(f, f_N^{k*}) &= \int_0^1 \text{Bias}(y)^2 dy + \int_0^1 \text{Variance}(y)dy \\
&= \left(\frac{\varepsilon^2}{12} \int_0^1 (f'(y))^2 dy + \mathcal{O}(\varepsilon^4) \right) + \left(\frac{1}{N\varepsilon} + \mathcal{O}(\varepsilon/N) + \mathcal{O}(1/N) \right) \\
&= \frac{\varepsilon^2}{12} \int_0^1 (f'(y))^2 dy + \frac{1}{N\varepsilon} + \mathcal{O}(\varepsilon^4) + \mathcal{O}(1/N). \quad \text{(assuming } \varepsilon/N \text{ is smaller than } 1/N)
\end{aligned}$$

Substituting $\varepsilon = 2^{-k}$:

$$R(f, f_N^{k*}) = \frac{2^{-2k}}{12} \int_0^1 (f'(y))^2 dy + \frac{2^k}{N} + \mathcal{O}(2^{-4k} + 1/N).$$

This gives the asymptotic risk. The $\mathcal{O}(2^{-4k} + 1/N)$ term is negligible, and can be disregarded. □

C Additional Related Work

Here, we provide additional methods for learning conditional distributions over $\mathbb{R}$ and their pros and cons compared to our proposed decoding-based method. While it may be interesting to more broadly benchmark these methods in the future, our main focus in this paper however, is to provide the technical layout for decoding-based regession and its general implications to language model training over numeric data as a whole. Furthermore, many of the methods below significantly increase the complexity and number of possible confounding factors, as they also modify the encoder. We emphasize the relative simplicity of our method which only requires changing the regression *head* and not the entire network body.

One general paradigm has been via stochastic networks, in which stochastic activations or weights are used to simulate multiple possible models. Very early works such as Sigmoid Belief Nets (Neal, 1992) later modified for learning conditional distributions (Tang & Salakhutdinov, 2013) were introduced but have not seen wide adoption due to their complex architectural modifications and expectation-maximization updates during training.

Bayesian neural networks (Lampinen & Vehtari, 2001; Titterington, 2004; Goan & Fookes, 2020) can be seen as more modern versions of the stochastic network approach, using additional techniques for architecture creation (e.g. graphical models) and Bayesian inference (Markov Chain Monte Carlo or variational inference). Similarly, Energy-based models (Teh et al., 2003) have been applied to regression (Gustafsson et al., 2020; Liu et al., 2022) where $p(y|x) \propto \exp(E(x, y))$ has been shown to work even for convolutional representations $\phi(x)$ over images, but has still seen limited use due their complex use of MCMC required at inference time.

D Exact Experimental Details

For all models, we sweeped the encoder (basic MLP with ReLU activation) by varying the number of layers within [2,3,4,5] and hidden units within [256, 512, 2048].

For x-normalization, we apply a mean and std scaling, i.e. $x \leftarrow (x - x_{mean})/x_{std}$ where x_{mean}, x_{std} are coordinate-wise mean and standard deviations over all x's in the training set. The preprocessed tensor is then fed directly into the encoder.

For y-normalization, we apply min/max linear scaling, i.e. $y \leftarrow (y - y_{min})/(y_{max} - y_{min})$ where y_{min}, y_{max} are computed from the training set. This is applicable to models representing $[0, 1]$ output range (i.e. Riemann and Normalized Decoder). For Pointwise and Mixture Density heads, we further apply a shift $y \leftarrow y - 0.5$ to center the values within $[-0.5, 0.5]$.

All models were trained with a maximum of 300 epochs. To prevent overfitting, we apply early stopping (patience=5) where the validation split is 0.1 on the training set. Adam learning rates were sweeped over [1e-4, 5e-4].

We further describe hyperparameters and sweeps for individual heads below:

Pointwise: Uses ReLU activations on every hidden layer.

- Weight decay: [0.0, 0.1, 1.0]

Unnormalized Decoder: Uses vanilla temperature sampling.

- Base B: [4, 8, 10]
- Exponent Digit Count E: [1, 2, 4]
- Mantissa Digit Count M: [2, 4, 8]
- Transformer size: (3 layers, 128 units, 4 heads) or (1 layer, 32 units, 1 head).

Normalized Decoder: Sampling same as unnormalized decoder.

- Base B: [2, 4, 8]
- Length K: [4, 8, 6]
- Transformer size: Same as unnormalized decoder.

Riemann/Histogram Distribution: We specify a bin count, which uniformly partitions the range $[0, 1]$ into equally spaced bins. Output is parameterized using softmax.

- Bin Count: [16, 64, 256, 1024, 4096, 16384]

Mixture Density Network: Given a mixture count M, the distribution head consists of mixture $\pi_M \in \triangle^M$, mean $\mu_M \in \mathbb{R}^M$, and standard deviation $\sigma_M \in \mathbb{R}^M$. Mixtures were parameterized using softmax, while standard deviations were via $\text{ELU}(x) + 1$ activation to enforce positivity.

- Mixtures M: [1, 2, 5, 10, 20, 50, 1000]